Available online at www.sciencedirect.com
SCIENCE DIRECT®
Journal of Membrane Science 261 (2005) 114–120
journal of MEMBRANE SCIENCE
www.elsevier.com/locate/memsci

Shell side mass transfer in a transverse flow hollow fiber membrane contactor

Ju-Meng Zheng [a,b], Zheng-Wei Dai [b], Fook-Sin Wong [a], Zhi-Kang Xu [b,*]

[a] *Institute of Environmental Science and Engineering, Nanyang Technological University, Innovation Center, Block 2, Unit 237, 18 Nanyang Drive, Singapore 637723, Singapore*
[b] *Institute of Polymer Science, Zhejiang University, Zheda Lu 38, Hangzhou 310027, PR China*

Received 27 February 2004; received in revised form 16 February 2005; accepted 16 February 2005
Available online 20 April 2005

Abstract

The free surface model was introduced to describe the shell side fluid flow in a transverse flow hollow fiber membrane contactor, and a new method was developed to calculate the shell side hydraulic diameter, the effective average velocity, and the Reynolds number. An empirical shell side mass transfer correlation was presented for commercial Liqui-Cel® Extra-Flow contactors on the basis of the experimental data reported by Sengupta et al. The data were correlated very well with maximum discrepancies of ±10% between the predicted and observed results.

Keywords: Membrane contactors; Transverse flow; Mass transfer; Hydrodynamics; Free surface model

1. Introduction

A membrane contactor is a device that achieves gas/liquid or liquid/liquid mass transfer without dispersion of one phase within another. This is accomplished by passing the fluids on the opposite sides of a microporous membrane. Through the careful control of the pressure difference between the fluids, one of the fluids is immobilized in the pores of the membrane so that the fluid/fluid interface is located at the mouth of each pore [1]. Usually, two types of modules, called *parallel flow* and *transverse* or *cross flow* are used. It has been reported that the transverse flow module has a number of advantages such as a larger shell side mass transfer coefficient, minimal flow channeling, better scale-up characteristics and more precise performance prediction [2]. The main features of the transverse flow module have been summarized by Gabelman and Hwang [1] and Sengupta et al. [2].

The most well-known transverse flow module, which is schematically shown in Fig. 1, is the Liqui-Cel® Extra-Flow module commercialized by CELGARD LLC (Charlotte, USA). Celgard® microporous polypropylene hollow fiber membranes used in this module have been woven into fabric to allow more uniform fiber spacing, which in turn leads to high mass transfer coefficient. The Extra-Flow module contains a central shell side baffle, a feature that offers two advantages: (1) the baffle can improve the mass transfer efficiency by minimizing shell side by-passing; (2) it provides a component of velocity normal to the membrane surfaces, which results in a higher mass transfer coefficient than that achieved with strictly parallel flow [2].

Generally, mass transfer in a hollow fiber contactor can be described using a resistance-in-series model [1]. The tube side mass transfer can be described with the Lévêque equation and the membrane resistance can be calculated from known membrane parameters such as membrane thickness, tortuosity and porosity. However, mass transfer correlation for shell side fluid flow has not been well established up to now. A conventional approach is to use the empirical correlation of the following form:

$$Sh = \alpha Re^{\beta} Sc^{0.33} \quad (1)$$

* Corresponding author. Tel.: +86 571 879 52605; fax: +86 571 879 51773.
E-mail address: xuzk@ipsm.zju.edu.cn (Z.-K. Xu).

0376-7388/$ – see front matter © 2005 Elsevier B.V. All rights reserved.
doi:10.1016/j.memsci.2005.02.035

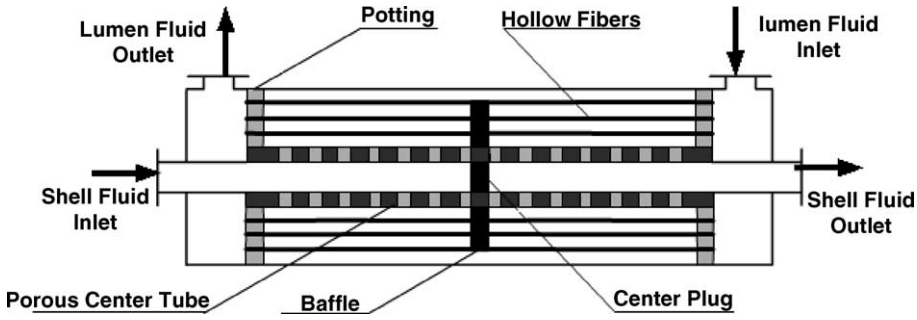

Fig. 1. Sketch of the Liqui-Cel® Extra-Flow membrane contactor (redrawn from Ref. [2]).

where the constants α and β are determined from experimental results. Based on this equation, some empirical correlations have been proposed for transverse flow modules [3–14]. However, there are only three correlations have been found applicable for commercial Liqui-Cel® Extra-Flow membrane contactors, as listed in Table 1. Among them, the correlations reported by Schöner et al. [10] and Baudot et al. [11] were derived directly from liquid–liquid extraction experiments using a 2.5 in. × 8 in. Liqui-Cel® Extra-Flow contactor. The correlation suggested by Kreith and Black [12], which was originally for a closely packed shell-and-tube heat exchanger, was found to give a good prediction of the shell side mass transfer coefficient in the Liqui-Cel® contactors in some studies [13,14]. Sengupta et al. [2] studied the shell side mass transfer in the large-scale application of membrane contactor for gas stripping with Liqui-Cel® modules. These investigations indicated that the shell side mass transfer coefficient is proportional to $Q^{0.38–0.45}$ (Q is the feed flow rate into the module) [2]. However, they did not present a correlation in the form of Eq. (1).

Besides, different methods were used for the calculation of the effective shell side velocity, the hydraulic diameter, and thus the Reynolds number [10–11,13–16]. This is due to the fact that there is no fundamental mathematical description of the shell side flow in a transverse flow contactor. Regarding to Seibert and Fair's work [17], the shell side flow was assumed to be perfectly mixed. However, as commented by Baudot et al. [11], this is not true for fluid flow through the fiber bundles.

In the literature, a method describing viscous flow relative to the arrays of solid rods is Happel's free surface model [18]. This model was developed on the basics that two concentric cylinders can serve as the model for fluid moving through an assemblage of cylinders. The inner cylinder consists of one of the rods in the assemblage and the outer cylinder of a fluid enveloped with a free surface [18]. In previous studies [19–21], the free surface model was adapted to describe the shell side fluid flow in a parallel flow hollow fiber membrane contactor. In fact, the free surface model can also be applied to the case of transverse flow [18]. The only difference is that, for the transverse flow, the boundary condition is that the fluid radial direction velocity (u_r), the fluid angular direction velocity (u_θ) and the free surface velocity (u_c) hold the following relationship at the free surface [18]:

$$u^2 = u_r^2 + u_\theta^2, \quad u_r = u\cos\theta, u_\theta = -u\sin\theta \tag{5}$$

The present work extends the idea of free surface model to the case of a transverse flow module. It is expected to derive expressions for the calculation of the shell side effective velocity and the hydraulic diameter, which can then be used to calculate the Reynolds number. It is also aimed to find an applicable correlation to predict the shell side mass transfer coefficients in the commercial Liqui-Cel® Extra-Flow membrane contactors. This part of the work is based on the experimental results reported by Sengupta et al. [2].

2. Theory

In order to study the shell side fluid flow in a transverse flow module, the fiber bundle was firstly divided into small, equally spaced cells with one fiber in each cell. And a free surface was presented at the imaginary cell boundary. It was assumed these flow cells are regularly arranged in layers between the center feed tube and the wall of the module. This means that the fiber number in the layer gradually increases from the layer near the center feed tube to the layer near the

Table 1
Mass transfer correlations for transverse flow modules

Correlation no.	Correlation	Brief conditions[a]	Reference
(2)	$Sh = 1.76Re^{0.82}Sc^{0.33}$	Feed flow rate 0.2–200 × 10^{-6} m^3/s	[10]
(3)	$Sh = 0.56Re^{0.62}Sc^{0.33}$	Feed flow rate 0.2–200 × 10^{-6} m^3/s	[11]
(4)	$Sh = 0.39Re^{0.59}Sc^{0.33}$[b]	Feed flow rate 10–50 × 10^{-6} m^3/s	[13]
		Feed flow rate 33 × 10^{-6} m^3/s	[14]

[a] Applied for Celgard Liqui-Cel® Extra-Flow 2.5 in. × 8 in. contactor.
[b] Kreith and Black equation, originally for a closely packed shell-and-tube heat exchanger [12].

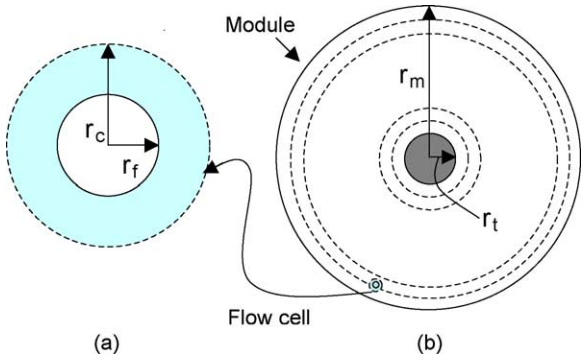

Fig. 2. Schematic representation for the flow cell: (a) in the cross-section division, (b) of module with free surface.

module wall. The division of module cross-section and the flow cell with free surface are sketched in Fig. 2.

The cell diameter (d_c) can be determined by assuming that the cell and the module have the same packing fraction:

$$d_c = \frac{d_f}{\sqrt{\varepsilon}} \tag{6}$$

where d_f is the outer diameter of the hollow fiber, ε is module packing fraction which can be calculated as:

$$\varepsilon = \frac{N d_f^2}{d_m^2 - d_t^2} \tag{7}$$

where d_m is the inner diameter of the module, d_t is the outer diameter of the center feed tube, and N is the total number of the hollow fibers.

In a transverse flows module, the feed fluid flows from the porous center tube passes through the fiber layer around the tube to the layer near the module wall. In each fiber layer, the total fluid flow is equally distributed between the cells. As a result, the local cell free surface velocity in each fiber layer is dependent on the number of fibers number in the layer. Therefore, the average cell free surface velocity ($u_{c,m}$) is defined as the free surface velocity in a layer, which has the log-mean number of the fibers. It has:

$$u_{c,m} = \frac{Q}{N_{lm}\pi d_c (l_{eff}/2)} \tag{8}$$

here Q is the feed flow, $l_{eff}/2$ is effective length of the module (the module is divided into two chambers by the baffle, Fig. 1); N_{lm} is the log-mean number of fibers in the fiber layer, defined as:

$$N_{lm} = \frac{N_{max} - N_{min}}{\ln(N_{max}/N_{min})} \tag{9}$$

where N_{max} is the number of fibers in the layer nearest to the module wall, and N_{min} is the number of fibers in the layer around the center feed tube:

$$N_{max} = \frac{d_m^2 - (d_m - d_c)^2}{d_f^2}\varepsilon \tag{10}$$

$$N_{min} = \frac{(d_t + d_c)^2 - d_t^2}{d_f^2}\varepsilon \tag{11}$$

For the flow cell, when the velocity in the free surface ($u_{c,m}$) is determined, we can calculate the effective cell velocity (also can be considered the effective shell side velocity, u_e) using the method proposed in Refs. [10,14]. It has:

$$\int u_e \, dr = \int \frac{Q}{N_{lm}} \frac{1}{2\pi(l_{eff}/2) jr} \, dr = \int \frac{u_{c,m} r_c}{r} \, dr \tag{12}$$

Integral Eq. (12) from fiber radius (r_f) to cell radius (r_c), the following relationship can be obtained as:

$$u_e = \frac{d_c \ln(d_f/d_c)}{d_f - d_c} u_{c,m} \tag{13}$$

Combining Eqs. (8)–(13), the effective cell velocity can be expressed as:

$$u_e = \frac{\ln \varepsilon}{4(\sqrt{\varepsilon} - 1)} \frac{\ln[(2d_m - d_c)/(2d_t + d_c)]}{(d_m - d_t - d_c)} \frac{Q}{\pi(l_{eff}/2)} \tag{14}$$

In order to calculate the Reynolds number, it still needs to know the hydraulic diameter (d_h). For the flow cell, the hydraulic diameter is defined as the ratio of four times the cross-sectional area to the wetted perimeter as usually done:

$$d_h = \frac{\text{four cell void volumes}}{\text{wetted surface of the cell}} = \frac{d_c^2 - d_f^2}{d_f} = \frac{1 - \varepsilon}{\varepsilon} d_f \tag{15}$$

Using Eqs. (14) and (15), the Reynolds number and the Sherwood number can be calculated in term of the following definitions:

$$R_e = \frac{d_h u_e \rho}{\mu} \tag{16}$$

$$Sh = \frac{k d_h}{D} = \frac{1 - \varepsilon}{\varepsilon} \frac{k d_f}{D} \tag{17}$$

Eqs. (14)–(17) incorporate all the parameters of the module (diameter of the module, diameter of the center feed tube, diameter of the fiber, effective length of the fiber and the packing fraction) that affect the shell side hydrodynamics. These will be helpful in developing a desirable empirical correlation to describe the shell side mass transfer coefficient in the transverse flow module.

3. Results and discussion

3.1. Methods for the calculation of shell side effective velocity

In the literatures, several methods have been reported for the calculation of hydraulic diameter and shell side effective velocity in the Liqui-Cel® Extra-Flow hollow fiber membrane contactors. There are mainly two equations have been used to calculate the effective shell side velocity. The first

one is that proposed by Schöner et al. [10]:

$$u_e = \frac{Q}{\pi(l_{eff}/2)} \frac{\ln(d_m/d_t)}{d_m - d_t} \quad (18)$$

The second one, suggested by Mahmud et al. [14], is a correction incorporating the module packing fraction (ε):

$$u_e = \frac{1}{1-\varepsilon} \frac{Q}{\pi(l_{eff}/2)} \frac{\ln(d_m/d_t)}{d_m - d_t} \quad (19)$$

In the present study, the effective shell side velocity was calculated with Eq. (14). Because the outer diameter of the hollow fiber and the diameter of the free surface are much smaller than the inner diameter of the module (d_m) and the outer diameter of the feed tube (d_t), Eq. (14) can be simplified as:

$$u_e = \frac{\ln \varepsilon}{4(\sqrt{\varepsilon} - 1)} \frac{\ln(d_m/d_t)}{(d_m - d_t)} \frac{Q}{\pi(l_{eff}/2)} \quad (20)$$

Comparing Eqs. (15)–(17), it can be found that these three equations describe in quite different ways for the influences of the module packing fraction on the effective shell side velocity. The discrepancy among these three equations is also illustrated in Fig. 3. In this figure, *Y*-coordinate is labeled as η, a dimensionless parameter defined as:

$$\eta = u_e \frac{\pi(l_{eff}/2)}{Q} \frac{d_m - d_t}{\ln(d_m/d_t)} \quad (21)$$

where u_e is calculated according to Eqs. (18)–(20) respectively.

Eq. (19) was derived on the assumption that there is no fiber in the module. As a result, it can be seen from Fig. 3 that, the module packing fraction does not affect the shell side effective velocity at all. Therefore, it is difficult to imagine that it (Eq. (19)) can be applied to the module packed with thousands upon thousands hollow fibers. On the other hand, Eq. (20) indicates that the effective shell side velocity increases with the increase of module packing fraction, and the velocity will become infinity ($\eta \to \infty$) when the module is extremely tightly packed ($\varepsilon \to \infty$). It seems that only the influence of the decrease in module void area, which caused by the increase of module packing fraction, on the effective shell side velocity is taken into consideration in Eq. (20). Whereas, these authors might overlook the resistance enhancement caused by the packing fraction increase.

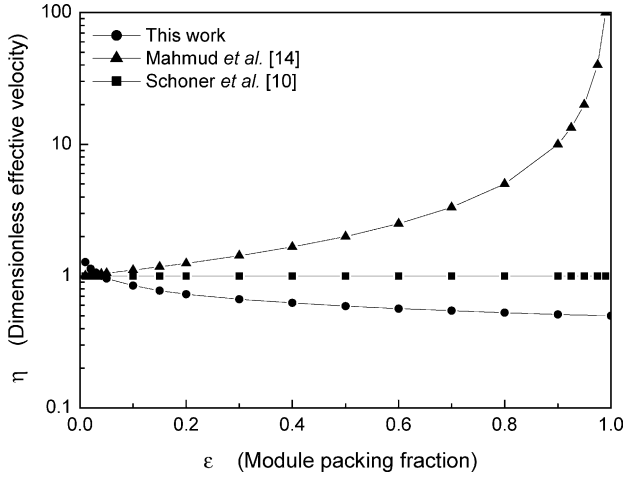

Fig. 3. Dimensionless shell side effective velocity defined with different methods.

The method developed in this work indicates that the effective shell side velocity decreases slightly with the increase of the module packing fraction, as shown in Fig. 3. This can be contributed to the combination of two factors: (1) the decrease of the module void area; and at the same time, (2) the fast increase of the flow resistance caused by the increase of the module packing fraction [18]. It also can be observed from Fig. 3 that, the dimensionless effective shell side velocity is slightly higher than 1 and this should not be the true. This result is due to that it was assumed that the cell diameter become infinity for $\varepsilon \to 0$ in model development (Eq. (6)).

3.2. Methods for the calculation of hydraulic diameter

In the studies of the shell side mass transfer, the Reynolds numbers have normally been calculated based on either the outer diameter of the fiber (d_f) [10,16] or the hydraulic diameter (d_h) [10,11]. And the hydraulic diameter can be calculated as:

$$d_h = \frac{d_m^2 - d_t^2 - N d_f^2}{N d_f} \quad (22)$$

As commented by Schöner et al. [10], the use of hydraulic diameter (in this case, the fiber bundle was treated as a packed bed of fibers) is more reasonable than the use of outer diameter. When introducing Eqs. (7) into (22), it can be found that Eq. (22) is the same as Eq. (15), which gives the definition of hydraulic diameter by the free surface model. It indicates that the method regarding the module as a packed bed of fibers and the free surface model deduce to the same definition of hydraulic diameter.

3.3. Shell side mass transfer correlation

Mass transfer in the shell side of transverse flow modules was studied by Sengupta et al. [2]. In their study, oxygen removal from water was performed in excess sweep conditions through Liqui-Cel® Extra-Flow contactors with various dimensions from lab scale to industrial using ones. It was found that the shell side mass transfer coefficient was proportional to $Q^{0.38–0.45}$ [2]. However, they did not present a mass transfer correlation. Here, the experimental results obtained by Sengupta et al. [2] were adopted to develop an empirical correlation for the shell side mass transfer in transverse flow module. Detailed specifications for the contactors used in their experiment work are listed in Table 2. The separation characteristics (oxygen removal rate, *E*) under various operating conditions (shell side feed flow, *Q*) are cited in Table 3. And then the overall mass transfer coefficients were

Table 2
Dimensional details for the Liqui-Cel® Extra-Flow contactors[a]

Nominal contactor size designator	Average cartridge i.d. (m)	Average cartridge o.d. (m)	Effective fiber length (m)	Fiber packing fraction	Total contactor area (based on fiber i.d.) (m^2)
2.5 × 8	0.022	0.050	0.16	0.45	1.2
4 × 28	0.032	0.088	0.62	0.43	14.9
4 × 13	0.032	0.085	0.25	0.43	5.7
10 × 28	0.114	0.245	0.61	0.43	103.8

[a] Nominal fiber inside diameter (i.d.) = 240×10^{-6} m; nominal fiber outside diameter (o.d.) = 300×10^{-6} m. All data were reported by Sengupta et al. [2].

calculated by the following equation [2]:

$$k = \frac{Q}{A} \ln \left[\frac{1}{1 - E} \right] \tag{23}$$

where A is the total contact area based on fiber inner diameter (Table 2). For the oxygen removal process in excess sweeping conditions, the main resistance to mass transfer is mainly located in the shell side. In other words, it is reasonable to assume the shell side mass transfer coefficient is equal to the overall mass transfer coefficient calculated by Eq. (23). Following this assumption, it is possible to get a shell side mass transfer correlation.

On the other hand, the shell side Reynolds number was calculated according to Eqs. (14)–(16) using the known data of feed flow (Table 3) and module dimensions (Table 2). Sherwood number was calculated using Eqs. (15) and (17) when the mass transfer coefficient was already calculated by Eq. (23). Results for the calculated Reynolds number and Sherwood number are also summarized in Table 3.

Further examination of the relationship between the Reynolds number and the Sherwood number reveals that the data can be correlated as follows:

$$Sh = 2.15 Re^{0.42} Sc^{0.33} \tag{24}$$

The correlation is valid in the Reynolds number from 0.8 to 20, subject to the experimental conditions (Table 3). Fig. 4 shows that this correlation relates with the experimental results very well. It can be seen that the maximum discrepancy between the correlation predictions and the experimental data is within 10%. This indicates that mass transfer data reported by Sengupta et al. [2] can be described by an empirical correlation that uses the definitions of the effective shell side velocity, hydraulic diameter, Reynolds number and Sherwood

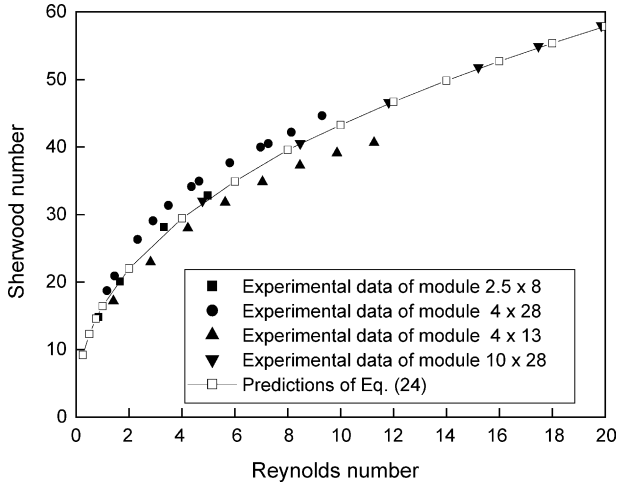

Fig. 4. Comparison of the shell side mass transfer predicted by the proposed correlation (Eq. (24)) to experimental data [2] for various Liqui-Cel® contactors.

Table 3
Experimental data [2] and calculated Reynolds number and Sherwood number

2.5 × 8 Contactor				4 × 28 Contactor				4 × 13 Contactor				10 × 28 Contactor			
Water flow[a] ($\times 10^6$ m/s)	Oxygen removal[a] (%)	Re^b	Sh^b	Water flow[a] ($\times 10^6$ m/s)	Oxygen removal[a] (%)	Re^b	Sh^b	Water flow[a] ($\times 10^6$ m/s)	Oxygen removal[a] (%)	Re^b	Sh^b	Water flow[a] ($\times 10^6$ m/s)	Oxygen removal[a] (%)	Re^b	Sh^b
32	96.14	0.842	14.85	252.3	99.68	1.162	18.72	126.2	98.48	1.410	17.20	3195	99.59	4.778	32.04
63	89.32	1.658	20.09	315.4	99.41	1.453	20.91	252.3	93.89	2.817	22.95	5665	97.90	8.471	39.92
126	79.12	3.317	28.15	504.7	98.24	2.324	26.32	378.5	89.68	4.226	27.98	7904	95.60	11.82	45.03
189	70.42	4.975	32.82	630.8	97.18	2.905	29.07	504.7	85.58	5.634	31.82	10168	93.39	15.21	50.39
				757.0	95.96	3.487	31.36	630.8	81.67	7.042	34.85	11689	91.38	17.48	52.27
				946.3	93.89	4.358	34.15	757.0	77.93	8.460	37.28	13279	89.54	19.86	54.69
				1009.3	93.15	4.648	34.94	883.2	74.37	9.860	39.13				
				1261.7	90.10	5.811	37.67	1009.3	70.97	11.27	40.64				
				1514.0	87.06	6.972	39.98								
				1577.7	86.33	7.263	40.52								
				1766.3	84.27	8.134	42.19								
				2018.7	81.97	9.297	44.65								

[a] Experimental data reported by Sengupta et al. [2].
[b] Calculated Reynolds number and Sherwood number with the correlations developed in this work.

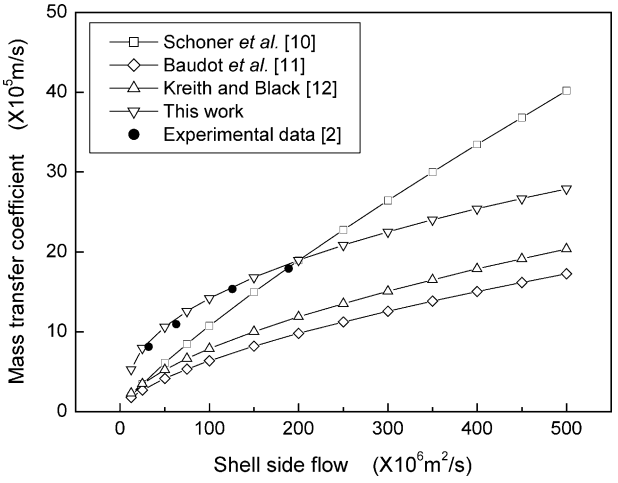

Fig. 5. Comparison of various correlations applied to the 2.5 in. × 8 in. Liqui-Cel® Extra-Flow contactor.

number developed in present study. Such correlation will be very helpful in the design of membrane contactor processes using Liqui-Cel® modules.

The Reynolds exponent in Eq. (24) is 0.42, which can well fit the experimental data ($k \propto Q^{0.38–0.45}$) reported by Sengupta et al. [2]. A value larger than 0.33 indicates that the transverse flow module provides a component of velocity perpendicular to the hollow fiber surface, which results in a higher mass transfer coefficient than that achieved with the parallel flow module. On the other hand, the value is lower than 0.66. It infers that the shell side flow cannot reach the turbulence flow in the tested Reynolds range (0.8–20). In the literatures, similar Reynolds exponents were also reported by Wickramasinghe et al. [3] ($Sh \propto Re^{0.47}$) and Wang et al. [4] ($Sh \propto Re^{0.46}$) for cross flow modules fabricated in their laboratories by wrapping hollow fiber fabric around a central pipe, as in the case of the commercial Liqui-Cel® Extra-Flow module [16].

The shell side mass transfer correlations listed in Table 1 were also used to fit the experimental data provided by Sengupta et al. [2]. The results are shown in Fig. 5. For comparison, the predictions by Eq. (24) are also shown in this figure.

It should be noticed that, in Kreith and Black's correlation, the shell side Reynolds number and the Sherwood number were defined in term of the fiber outer diameter. The shell side effective velocity was calculated by Eq. (19). In the correlations of Schöner et al. and Baudot et al., the shell side effective velocity and the hydraulics diameter are calculated by Eqs. (18) and (22) respectively. As a result, in Fig. 5, X and Y coordinates were labeled as feed flow (Q) (but not the Reynolds number), mass transfer coefficient (k) (but not the Sherwood number) respectively. Besides, in Fig. 5, the equation of Schöner et al. was modified from its original form, because the authors used the pore area but not the whole membrane surface as the contact area, and it would lead to high mass transfer coefficients as pointed in the literatures [11,16]. Therefore, the correlation suggested by Schöner et al. was corrected with the membrane surface porosity (γ) as follows when it was plotted in Fig. 5:

$$Sh = 1.76\gamma Re^{0.82} Sc^{0.33} \quad (25)$$

It can be seen from Fig. 5 that, except the correlation proposed by Schöner et al., the shell side mass transfer coefficients show similar Reynolds exponent dependency in other three correlations. On the other hand, the correlations of Schöner et al. [10], Baudot et al. [11] and Kreith and Black [12] predict lower mass transfer coefficient than that observed by experiments [2]. More recently, in the study of liquid–liquid extraction with Liqui-Cel® Extra-Flow contactor, Soldenhoff et al. [16] found that the experimental overall mass transfer coefficients were much lower than the predicted values. The prediction was performed with the conventional resistance-in-series model, where the shell side mass transfer was estimated with the correlation proposed by Baudot et al. [11], and the tube side mass transfer with Lévêque equation. The authors stated that the difference is due to the contribution of extraction chemical kinetics at or very close to the interface [16]. Whatever, we think the mass transfer in a liquid–liquid extraction is more complex than that in a gas stripping or absorption process. In other words, it is much easier to reach the condition that the overall mass transfer coefficient is equal to the shell side mass transfer in a gas stripping or absorption process and thus it is a suitable system for the study of the complex shell side mass transfer.

4. Conclusions

Free surface model was applied to describe the shell side flow in a transverse flow hollow fiber membrane contactor. Based on this, a method was developed to calculate the shell side hydraulic diameter, the effective shell side velocity and the Reynolds number. An empirical correlation was proposed to relate with the mass transfer data (oxygen stripping in excess sweep conditions) reported by Sengupta et al. [2]. The discrepancies between the correlation predictions and experimental data were within 10%. Additionally, it was shown that the correlation come out from liquid–liquid extraction predicts lower shell side mass transfer coefficients than that obtained by experiments. It indicates that gas stripping or absorption experiment is a suitable system for the study of the complex shell mass transfer, where we can easily reach the condition that the overall mass transfer coefficient is mainly located in the shell side.

Acknowledgements

The authors gratefully acknowledge the support from Agency of Science, Technology and Research of Singapore (A*STAR) to fund the IESE program.

Nomenclature

A	total contact area offered by the membrane contactor (m^2)
d_c	diameter of the cell (m)
d_f	fiber outer diameter (m)
d_h	hydraulic diameter (m)
d_m	inside diameter of the cartridge (m)
d_t	outside diameter of the center feed tube (m)
D	diffusion coefficient (m^2/s)
k	shell side mass transfer coefficient (m/s)
l_{eff}	effective length of the fiber (m)
N	total number of the fibers
N_{lm}	log-mean number of the fibers in fibers layer
N_{max}	number of the fibers in the layer nearest to the wall
N_{min}	number of the fibers in the layer nearest to the feed tube
Q	volumetric flow rate of shell side (m^3/s)
r_c	free surface radius (m)
r_f	fiber radius (m)
$u_{c,m}$	average cell free surface velocity (m/s)
u_e	effective shell side velocity (m/s)
u_r	radial direction velocity (m/s)
u_θ	angular direction velocity (m/s)

Greek letters

α,β	constants in Eq. (1)
γ	membrane porosity
η	dimensionless shell side effective velocity, Eq. (21)
ε	module packing fraction
μ	viscosity of shell side liquid (Pa s)
ρ	density of shell side liquid (kg/m^3)

References

[1] A. Gabelman, S.-T. Hwang, Hollow fiber membrane contactors, J. Membr. Sci. 159 (1999) 61–106.

[2] A. Sengupta, P.A. Peterson, B.D. Miller, J. Schneider, C.W. Fulk Jr., Large-scale application of membrane contactors for gas transfer from or to ultrapure water, Sep. Purif. Technol. 14 (1998) 189–200.

[3] S.R. Wickramasinghe, M.T. Semmens, E.L. Cussler, Mass transfer in various hollow fiber geometries, J. Membr. Sci. 84 (1993) 1–14.

[4] K.L. Wang, E.L. Cussler, Baffled membrane modules made with hollow fiber fabric, J. Membr. Sci. 85 (1993) 265–278.

[5] M.-C. Yang, E.L. Cussler, Designing hollow fiber contactors, AIChE J. 32 (1986) 1910–1915.

[6] P. Cota, T.-L. Bersillon, A. Hugard, Bubble-free aeration using membrane: mass transfer analysis, J. Membr. Sci. 47 (1989) 91–106.

[7] T. Ahmed, M.J. Semmens, Use of transverse flow hollow fiber for bubbleless membrane aeration, Water Res. 30 (1996) 440–446.

[8] D.W. Johnson, M.J. Semmens, J.S. Gulliver, Diffusive transport across unconfined hollow fiber membrane, J. Membr. Sci. 128 (1997) 67–81.

[9] D. Bhaumik, S. Majumdar, K.K. Sirkar, Absorption of CO_2 in a transverse flow hollow fiber membrane module having a few wraps of the fiber mat, J. Membr. Sci. 138 (1998) 77–82.

[10] P. Schöner, P. Plucinske, W. Nitsch, U. Daiminger, Mass transfer in the shell side of cross flow hollow fiber modules, Chem. Eng. Sci. 53 (13) (1998) 2316–2319.

[11] A. Baudot, J. Floury, H.E. Smoreburg, Liquid–liquid extraction of aroma compound with hollow fiber contactor, AIChE J. 47 (2001) 1780–1793.

[12] F. Kreith, W.Z. Black, Basic Heat Transfer, Harper & Row, New York, 1980.

[13] F.-X. Pierre, I. Souchon, V. Athes-Dutour, M. Marin, Membrane-based solvent extraction of sulfur aroma compounds: influence of operating conditions on mass transfer coefficients in a hollow fiber contactor, Desalination 148 (2002) 199–204.

[14] H. Mahmud, A. Kumar, R.M. Narbaitz, T. Matsuura, A study of mass transfer in the membrane air-stripping process using microporous polypropylene hollow fibers, J. Membr. Sci. 179 (2000) 29–41.

[15] M.J. Gonzalez-Munoz, S. Luque, J.R. Alvarez, J. Coca, Recovery of phenol from aqueous solutions using hollow fiber contactors, J. Membr. Sci. 213 (2003) 181–193.

[16] K. Soldenhoff, M. Shamieh, A. Manis, Liquid–liquid extraction of cobalt with hollow fiber contactor, J. Membr. Sci. 252 (2005) 183–194.

[17] A.F. Seibert, J.R. Fair, Scale-up of hollow fiber exactors, Sep. Sci. Technol. 32 (1997) 573–583.

[18] J. Happel, Viscous flow relative to arrays of cylinders, AIChE J. 5 (1959) 174–179.

[19] J.-M. Zheng, Y.-Y. Xu, Z.-K. Xu, Flow distribution in randomly packed hollow fiber membrane module, J. Membr. Sci. 211 (2003) 263–269.

[20] J.-M. Zheng, Y.-Y. Xu, Z.-K. Xu, Shell side mass transfer characteristics in a parallel flow hollow fiber membrane module, Sep. Sci. Technol. 38 (2003) 1247–1267.

[21] S. Karoor, K.K. Sirkar, Gas absorption studies in microporous hollow fiber membrane modules, Ind. Eng. Chem. Res. 32 (1993) 674–684.